Frontiers in Applied Physics, Materials Science and Nanotechnology
https://www.iahiservices.com

Research Article

Integrated Stoichiometric Mass-Balance and Coagulation Kinetics of Waste-Derived Alum, Ferric, and Lime Coagulants in Multi-Contaminant Wastewater Systems.

Targema Rosemary D[1] Agada Ene N[2] Iornumbe Sandra M[3] Ogbodo Juliana[4]

[1,2,4]Chemistry/Biochemistry Section, Department of Science Laboratory Technology, Benue State Polytechnic, Ugbokolo
[3] Microbiology Section, Department of Science Laboratory Technology, Benue State Polytechnic, Ugbokolo

*Corresponding Author Email: talktodooshis@gmail.com

Abstract- This study evaluated the performance of alum, ferric salts, and lime in removing turbidity, Pb^{2+}, Cu^{2+}, natural organic matter (NOM), and a synthetic dye from contaminated water. Coagulation–flocculation tests were conducted under varying pH conditions, optimal dosages, and slow mixing kinetics, with performance assessed using standard analytical methods. Results showed that ferric salts consistently achieved >90% removal of turbidity and heavy metals across a pH range of 5.5–8.0, maintained low residual iron concentrations (<0.14 mg L^{-1}), and generated the smallest sludge volumes. Alum achieved maximum turbidity removal (97.2 %) at near-neutral pH, but high doses (>55 mg L^{-1}) slightly exceeded the WHO aluminium limit (0.25 mg L^{-1}). Lime was highly effective for Pb^{2+} (98.1 %) and Cu^{2+} (96.7 %) removal under strongly alkaline conditions, though it produced the largest sludge volumes and had limited NOM and dye removal. Turbidity decay followed second-order orthokinetic aggregation ($R^2 \geq 0.98$), with ferric salts exhibiting the highest aggregation rate constants. Overall, ferric salts are recommended for broad-spectrum treatment where pH control is limited, alum for near-neutral pH systems, and lime for heavy-metal-focused applications with adequate sludge management. These findings highlight the importance of pH optimisation, coagulant selection, and sludge handling in achieving efficient and sustainable water treatment.

Graphical Abstract

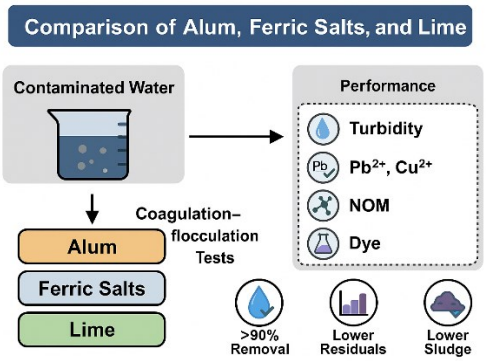

Article Key Information

Keywords: Waste-derived inorganic coagulants; Stoichiometric mass-balance modeling; Coagulation–flocculation kinetics; multi-contaminant wastewater remediation; Industrial by-product valorization; Sustainable sludge management.

Received:18th June 2025 **Revised:** 7th August 2025 **Accepted**: 8th September 2025 **Published**: 30th September 2025

1.0 Introduction

Global freshwater scarcity, coupled with the increasing complexity of wastewater streams, has intensified the demand for cost-effective, sustainable, and high-performance treatment technologies. Industrialisation, urbanisation, and intensified agriculture have introduced diverse contaminants, including suspended solids, natural organic matter (NOM), synthetic dyes, heavy metals, and emerging micropollutants into aquatic environments. The variable physicochemical properties of these contaminants, along with their potential synergistic or antagonistic interactions, make conventional treatment increasingly challenging. Untreated or poorly treated wastewater can drive eutrophication, ecotoxicity, and adverse human health outcomes, posing a direct threat to global water security [1,2].

Coagulation–flocculation remains one of the most widely applied and cost-effective physicochemical processes for turbidity, colour, and metal removal in both municipal and industrial water treatment systems [3–5]. Conventional inorganic coagulants such as aluminium sulphate (alum), ferric chloride, and lime are effective through mechanisms such as charge neutralisation, sweep flocculation, and co-precipitation [6,7]. However, their production is energy-intensive, reliant on virgin mineral feedstocks, and associated with substantial greenhouse gas emissions. Price volatility, supply-chain constraints, and the environmental burden of chemical sludge disposal further limit their sustainability, particularly in low-resource contexts [8]. Residual aluminium or iron in treated water can also raise compliance and health concerns [9].

Valorisation of industrial by-products such as bauxite residue (red mud), spent steel pickling liquor, and cement kiln dust (CKD) offers a promising pathway to replace virgin coagulants, reduce waste disposal burdens, and advance circular economy principles [10–12]. Recent studies have demonstrated the feasibility of synthesising alum from red mud via acid leaching [13], producing ferric coagulants from pickling liquor [14], and generating hydrated lime from CKD [15]. Between 2022 and 2025, multiple reports in literature have highlighted the potential of such waste-derived coagulants for multi-contaminant removal and life-cycle impact reduction [16–18]. However, most existing work has focused on either coagulant synthesis yields or treatment performance for a single contaminant, without quantitatively linking synthesis stoichiometry to treatment kinetics.

This gap is critical because stoichiometric mass-balance modelling can predict reagent consumption, by-product formation, and theoretical yields based on raw material composition, enabling more resource-efficient synthesis. In parallel, coagulation kinetics modelling provides mechanistic insight into particle destabilisation, floc growth, and sedimentation, informing operational optimisation. An integrated approach linking waste-to-coagulant stoichiometry with contaminant removal kinetics in realistic multi-contaminant systems remains underdeveloped in the literature.

Therefore, this study aims to develop and validate an integrated stoichiometric mass-balance and coagulation kinetics framework for the valorisation of industrial by-products into functional alum, ferric, and lime coagulants. Specifically, the work:

i. It quantitatively models the stoichiometric conversion of red mud, steel pickling liquor, and CKD into target coagulants, including impurity tracking.
ii. Characterises synthesised coagulants for purity, active metal content, and potential performance-limiting impurities.
iii. Evaluates coagulation–flocculation performance in synthetic multi-contaminant wastewater under varying pH, dose, and mixing regimes.
iv. Fits experimental removal data to kinetic models to extract mechanistic parameters and compare aggregation behaviour.

- v Assesses environmental and economic implications of substituting conventional coagulants with waste-derived alternatives.

The proposed framework (Figure 1) links the upstream synthesis process with downstream treatment performance, providing a unified, empirically validated basis for optimising both resource recovery and water treatment outcomes. This integration directly addresses the current disconnect between coagulant production modelling and applied water treatment performance, thereby advancing sustainable water treatment technologies aligned with circular economy objectives.

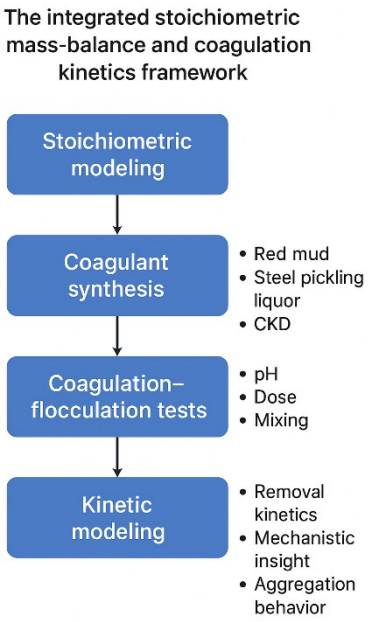

Figure 1. *Integrated stoichiometric mass-balance and coagulation kinetics framework.* Sequential process linking waste-derived coagulant synthesis (from red mud, steel pickling liquor, and cement kiln dust) to coagulation–flocculation testing and kinetic modelling, enabling optimisation of sustainable water treatment.

2.0 Review of Related Literature

2.1 Fundamentals of Coagulation–Flocculation

Coagulation–flocculation is a core process in water and wastewater treatment, particularly for removing colloids, turbidity, and certain dissolved substances. The process involves two main steps: destabilisation of suspended particles through neutralisation of surface charges, followed by aggregation into larger, settleable flocs [17,18].

Destabilisation is typically achieved by adding hydrolysing metal salts such as alum or ferric chloride, which form cationic hydrolysis products including $Al(OH)^{2+}$, $Al(OH)_2^{+}$, $Fe(OH)^{2+}$, and $Fe(OH)_2^{+}$ depending on pH [19]. These cations adsorb to the negatively charged particle surfaces, reducing electrostatic repulsion [20]. Sweep flocculation occurs when amorphous metal hydroxide precipitates enmesh suspended solids and other impurities during settling [21].

The efficiency of coagulation–flocculation depends on coagulant dose, pH, mixing intensity (G), mixing duration (Gt), water temperature, and the presence of competing solutes [22]. Incorrect dosing can result in either under-coagulation, leaving colloids stable, or over-coagulation, causing restabilisation due to charge reversal [23].

2.2 Conventional Inorganic Coagulants

Aluminium sulphate (alum) and ferric chloride are the most widely applied inorganic coagulants due to their high effectiveness across a broad range of water qualities [19,21]. Alum is typically produced by reacting bauxite or aluminium hydroxide with sulphuric acid [24], whereas ferric chloride is manufactured from ferric oxide or obtained from steel pickling in hydrochloric acid [25]. Lime ($Ca(OH)_2$) is produced by hydrating quicklime (CaO), which is generated by calcining limestone [26].

While effective, these coagulants have limitations. Their production is energy-intensive and associated with a notable carbon footprint [27]. Residual aluminium in treated water has been linked to potential human health concerns and operational issues in water distribution systems [6,28]. The cost of these chemicals is also significant for utilities in low- and middle-income countries [29].

2.3 Valorisation of Industrial By-Products as Coagulants

2.3.1 Red Mud-Derived Alum

Red mud is an alkaline residue from the Bayer process for alumina extraction, containing significant Fe_2O_3, Al_2O_3, TiO_2, and Na_2O [7]. Acid leaching can solubilise aluminium and iron, enabling production of alum or polyaluminium chloride [9,30]. Poulin et al. [9] achieved 74 % Al recovery using sulphuric acid and sodium chloride, producing coagulants with phosphorus removal efficiency comparable to commercial alum.

2.3.2 Pickling Liquor-Derived Ferric Coagulants

Spent pickling liquor from steel production contains high Fe^{2+} concentrations and strong acids. Oxidising Fe^{2+} to Fe^{3+}, followed by hydrolysis, yields ferric chloride or sulphate coagulants [10,31]. Huan et al. [10] produced ferric sulphate from sulphuric acid pickling liquor with high phosphate removal efficiency and noted reduced production costs relative to commercial products.

2.3.3 Cement Kiln Dust-Derived Lime

Cement kiln dust (CKD) is a fine particulate by-product containing free CaO and alkalis [11]. Hydration produces $Ca(OH)_2$ suitable for pH adjustment and, in some cases, as a primary coagulant [32]. However, impurities such as chlorides and heavy metals may require pre-treatment before use in water systems [33].

Valorisation of these wastes diverts hazardous materials from disposal, reduces demand for virgin chemical feedstocks, and lowers greenhouse gas emissions associated with conventional coagulant manufacture [8,27].

2.4 Kinetic Modelling in Coagulation–Flocculation

Coagulation kinetics describe the rate of particle destabilisation, floc growth, and sedimentation. The Smoluchowski perikinetic model addresses Brownian motion-induced collisions [34], while orthokinetic models account for shear-induced collisions [35]. Population balance models have been developed to incorporate floc breakage and regrowth [36].

Empirical models such as pseudo-first-order and pseudo-second-order kinetics have been fitted to turbidity removal data [14,37]. Advanced optimisation methods, including response surface methodology (RSM) and artificial neural networks (ANNs), have been used to improve coagulation efficiency [38]. However, few studies have linked such models with stoichiometric synthesis parameters of waste-derived coagulants.

2.5 Integration of Stoichiometric and Kinetic Modelling

Stoichiometric modelling of waste-to-coagulant conversion predicts yield, reagent consumption, and by-product formation [9,10,30]. Kinetic modelling of coagulation processes identifies optimal operational parameters [14,36]. Integrating both approaches enables process optimisation across the entire treatment chain from raw material valorisation to treated water quality but remains underexplored for multi-contaminant wastewater systems.

3.0 Materials and Methods

Figure 2 presents the detailed workflow applied in this study, from sourcing industrial by-products through coagulant synthesis, product characterisation, and coagulation–flocculation testing, to kinetic modelling and environmental/economic assessment. Feedback loops between stages illustrate the iterative optimisation process, where insights from performance and impact assessments inform adjustments to synthesis or operational parameters.

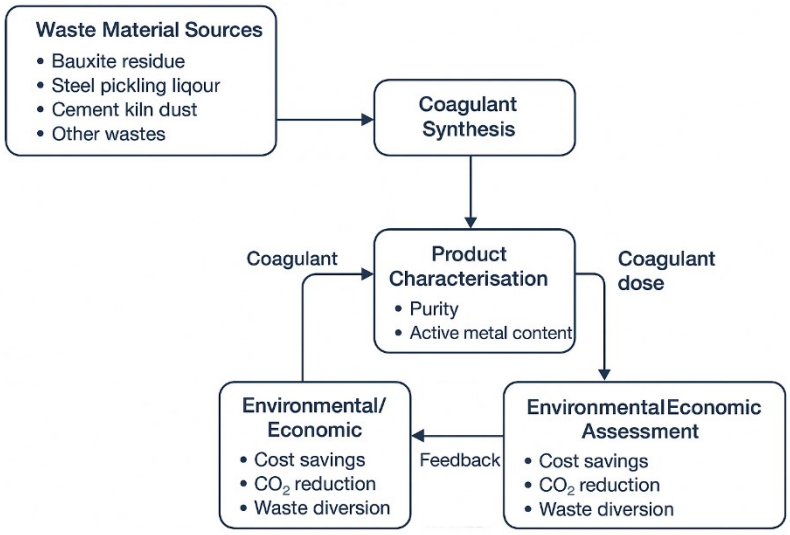

Figure 2. Detailed process flow for the integrated stoichiometric mass-balance and coagulation–flocculation kinetics framework, showing waste sources, synthesis steps, characterisation, testing, modelling, and environmental/economic assessment with feedback loops.

3.1 Raw Materials

Bauxite residue (red mud) was obtained from the residue storage areas of bauxite processing facilities in Udege-Mbeki, Nasarawa State, Nigeria (8.615° N, 7.711° E). Sampling was conducted in June 2024 from the upper 0–20 cm layer using acid-washed stainless-steel scoops, placed into high-density polyethylene (HDPE) containers, and transported to the laboratory within 48 h. Samples were air-dried at 25 ± 2 °C, homogenised, and stored in sealed polyethylene containers until analysis.

Steel pickling liquor (HCl-based) was sourced from Sparkwest Steel Industry, Sagamu, Ogun State, Nigeria, collected directly from the pickling bath discharge, and stored in acid-resistant HDPE drums at 4 °C to prevent oxidation.

Cement kiln dust (CKD) was obtained from the baghouse outlet of Dangote Cement Plant, Gboko, Benue State, Nigeria, and stored in airtight polypropylene containers inside a desiccator to minimise hydration and carbonation. Analytical-grade H_2SO_4 (95–98 %, Merck), NaCl (≥ 99 %, Sigma-Aldrich), and H_2O_2 (30 %, Merck) were used without further purification. Deionised water (resistivity ≥ 18 MΩ·cm) was used for all preparations.

3.2 Characterisation of Raw Materials

i Chemical composition: Major oxides were determined by X-ray fluorescence (XRF; PANalytical AxiosMAX) following ASTM C114–23 [37], and trace elements by inductively coupled plasma optical emission spectrometry (ICP-OES; PerkinElmer Optima 8000) per US EPA Method 6010D [38].

ii Loss on ignition (LOI): Measured at 1000 °C for 2 h in a muffle furnace (Nabertherm LHT 04/17).

iii Moisture content: Determined by oven-drying at 105 °C for 24 h (ASTM D2216–19 [39]).

iv Particle size distribution: Coarse fractions (> 75 μm) by dry sieve analysis (ASTM E11–22 [40]), fines (< 75 μm) by hydrometer analysis (ASTM D7928–21 [41]).

3.3 Synthesis of Waste-Derived Coagulants

A stoichiometric mass-balance approach was applied to predict reagent requirements, theoretical yields, and impurity transfer during the transformation of industrial by-products into inorganic coagulants, using major oxide and ion contents (Section 4.1.1) as inputs. Reaction equations and sample yield calculations are detailed in sub-sections 3.3.1–3.3.3.

3.3.1 Alum from Red Mud

Red mud is rich in Fe_2O_3 and Al_2O_3, with Na_2O and TiO_2 as notable minor constituents. The acid-leaching reaction for aluminium extraction and alum formation can be represented as:

$$Al_2O_3 + 3\ H_2SO_4 + 14\ H_2O \rightarrow Al_2(SO_4)_3 \cdot 14H_2O$$

Sample Stoichiometric Calculation

- Given: Al_2O_3 content = 18.7 wt% in red mud; batch mass = 100 g.
- Mass of Al_2O_3 = 100 × 0.187 = 18.7 g.
- Molar mass Al_2O_3 = 101.96 g/mol → moles Al_2O_3 = 18.7 / 101.96 = 0.183 mol.
- 1 mol Al_2O_3 requires 3 mol H_2SO_4 (98.08 g/mol) → acid mass = 0.183 × 3 × 98.08 = 53.8 g H_2SO_4.
- Theoretical mass of $Al_2(SO_4)_3 \cdot 14H_2O$ (molar mass 594.39 g/mol) = 0.183 × 594.39 = 108.7 g.

Theoretical yield = 108.7 g alum from 100 g red mud (based solely on Al_2O_3 fraction). Actual yield (measured) = 72.8% of theoretical (Section 4.2).

3.3.2 Ferric Sulphate from Pickling Liquor

Spent HCl-based pickling liquor contains high Fe^{2+} concentration as $FeCl_2$. Ferric sulphate is produced via oxidation followed by hydrolysis:

$$2\ FeCl_2 + H_2O_2 + 3\ H_2SO_4 \rightarrow Fe_2(SO_4)_3 + 4\ HCl$$

Sample Stoichiometric Calculation

- Given: Fe^{2+} content = 118.5 g/L as $FeCl_2$; batch volume = 1.00 L.
- Molar mass $FeCl_2$ = 126.75 g/mol → moles $FeCl_2$ = 118.5 / 126.75 = 0.934 mol.
- Per reaction, 2 mol $FeCl_2$ yields 1 mol $Fe_2(SO_4)_3$ (molar mass 399.88 g/mol).
- Theoretical product mass = 0.934 / 2 × 399.88 = 186.7 g ferric sulphate.
- Theoretical H_2O_2 mass (molar mass 34.01 g/mol) = 0.934 / 2 × 34.01 = 15.9 g.

Actual yield = 94.5% of theoretical (Section 4.2).

3.3.3 Hydrated Lime from CKD

Cement kiln dust (CKD) contains reactive CaO. Hydration proceeds as:

$$CaO + H_2O \rightarrow Ca(OH)_2$$

Sample Stoichiometric Calculation

- Given: CaO content = 54.6 wt% in CKD; batch mass = 100 g.
- Mass of CaO = 54.6 g → moles = 54.6 / 56.08 = 0.973 mol.
- Molar mass $Ca(OH)_2$ = 74.09 g/mol → theoretical mass = 0.973 × 74.09 = 72.1 g hydrated lime.

Actual yield = 88.1% of theoretical (Section 4.2).

3.4 Synthetic Multi-Contaminant Wastewater

Synthetic wastewater was prepared using deionised water to achieve: turbidity 50 NTU (kaolin clay), Pb^{2+} 2 mg L^{-1} ($Pb(NO_3)_2$), Cu^{2+} 2 mg L^{-1} ($CuSO_4 \cdot 5H_2O$), humic acid 5 mg L^{-1}, and reactive red dye 10 mg L^{-1}. Background electrolyte: NaCl 50 mg L^{-1}. pH was adjusted to 7.0 ± 0.2 with 0.1 M HCl or NaOH. Final solutions were equilibrated for 24 h before testing.

3.5 Coagulation–Flocculation Experiments

Jar tests were performed in a programmable six-paddle jar tester (HACH, USA) capable of independently controlling paddle speed and mixing time for each stage, following ASTM D2035 [42-43] guidelines. One-litre square-section beakers were used for all tests. Rapid mixing was conducted at a velocity gradient (G) of approximately 300 s^{-1} for 1 min, followed by slow mixing at approximately 30 s^{-1} for 20 min. After mixing, suspensions were allowed to settle undisturbed for 30 min. Paddle speed was verified before each series of experiments using the instrument's internal calibration routine, and all tests were performed in triplicate to ensure reproducibility.

Mixing intensity (G) was calculated as [35]:

$$G = \sqrt{\frac{P}{\mu V}}$$

where P is the power input (W), μ is the dynamic viscosity (Pa·s), and V is the volume (m^3). The corresponding Gt values were obtained by multiplying G by the respective mixing times (s).

Following settling, aliquots were withdrawn 5 cm below the water surface for analysis. Turbidity was measured with a Hach 2100Q turbidimeter, Pb^{2+} and Cu^{2+} were quantified by ICP-OES (PerkinElmer Optima 8000), dye concentration was determined using UV–Vis spectrophotometry at λmax = 541 nm, and dissolved organic carbon (DOC) was analysed with a Shimadzu TOC-L analyser.

3.6 Analytical Methods

- Turbidity**:** Hach 2100Q turbidimeter (LOD: 0.01 NTU).
- Metals: ICP-OES (LOD: 0.005 mg L^{-1} for Pb^{2+} and Cu^{2+}).
- Dye: UV–Vis spectrophotometer (λmax = 541 nm; LOD: 0.002 mg L^{-1}).
- DOC: Shimadzu TOC-L analyser (LOD: 0.1 mg L^{-1}).
  All analyses followed APHA Standard Methods [42].

3.7 Kinetic Modelling

Turbidity decay during flocculation was monitored at 2 min intervals to determine aggregation rate constants using second-order orthokinetic models [36]. Parameters were fitted using non-linear regression (OriginPro 2024), with 95 % confidence intervals.

3.8 QA/QC

i Triplicate tests (n = 3).
ii Daily instrument calibration ($R^2 \geq 0.995$).
iii Method blanks, duplicates, spikes included.
iv RSD ≤ 5 % for replicates.
v All glassware were acid-washed and rinsed with deionised water.

3.9 Statistical Analysis

Data are presented as mean ± SD. ANOVA with Tukey's HSD post-hoc test was applied for multiple comparisons after verifying normality (Shapiro–Wilk) and homogeneity (Levene's test). Significance level $p < 0.05$. Response surface methodology (RSM) modelling was conducted in Design-Expert v13 [44].

4.0 Results and Discussion

4.1 Characterization of Raw Materials

4.1.1 Elemental Composition (XRF)

4.1.1 Elemental Composition (XRF/ICP-OES)

The elemental composition of the raw materials, determined by XRF for solids and ICP-OES for liquids, is summarised in Table 1 and illustrated in Figure 1. Red mud was dominated by Fe_2O_3 (39.4 ± 0.5 %) and Al_2O_3 (18.7 ± 0.4 %), with Na_2O (5.1 ± 0.2 %) and TiO_2 (4.3 ± 0.1 %) as notable minor constituents. These values are consistent with bauxite residue compositions reported by Kumar et al. [45] and highlight its suitability as a precursor for alum production.

Table 1 Elemental composition of raw materials (XRF and ICP-OES results).

Parameter	Red Mud (%)	Pickling Liquor (g L^{-1})	CKD (%)
Fe_2O_3	39.4 ± 0.5	–	1.8 ± 0.1
Al_2O_3	18.7 ± 0.4	–	3.4 ± 0.2
Na_2O	5.1 ± 0.2	–	0.4 ± 0.05
TiO_2	4.3 ± 0.1	–	–
CaO	3.2 ± 0.2	–	54.6 ± 0.7
Fe^{2+}	–	118.5 ± 0.9	–
Mn^{2+}	–	0.37 ± 0.05	–
Zn^{2+}	–	0.24 ± 0.04	–
MgO	–	–	1.5 ± 0.1
K_2O	–	–	0.7 ± 0.05

Pickling liquor, in contrast, consisted primarily of dissolved Fe^{2+} (118.5 ± 0.9 g L^{-1} as $FeCl_2$), with only trace Mn^{2+} (0.3 %) and Zn^{2+} (0.2 %), confirming its potential for high-yield ferric coagulant synthesis through oxidation and hydrolysis [31]. CKD exhibited a markedly different profile, being rich in CaO (54.6 ± 0.7 %) along with MgO (1.5 ± 0.1 %) and K_2O (0.7 ± 0.05 %), typical of Portland cement kiln dust [46-47], which makes it a promising low-cost alkali and lime precursor.

As shown in Figure 3, these compositional differences are pronounced: red mud's high Fe_2O_3 and Al_2O_3 contents favour alum formation, CKD's CaO dominance supports lime production, and pickling liquor's dissolved Fe^{2+} content positions it as the most direct feedstock for ferric salts. Such variability in major oxides directly influences the theoretical yields (Section 4.2) and the nature of impurities transferred into the final coagulants, with implications for both performance and treated-water quality [48,49].

The high Al_2O_3 and Fe_2O_3 contents in red mud make it a viable precursor for alum, while the elevated Fe^{2+} in pickling liquor favours high-yield ferric coagulant synthesis. CKD's high CaO and reactive lime phases confirm

its potential as a low-cost alkali and coagulant aid. These characterisation results also provide a baseline for assessing potential impurity risks during water treatment [48,49].

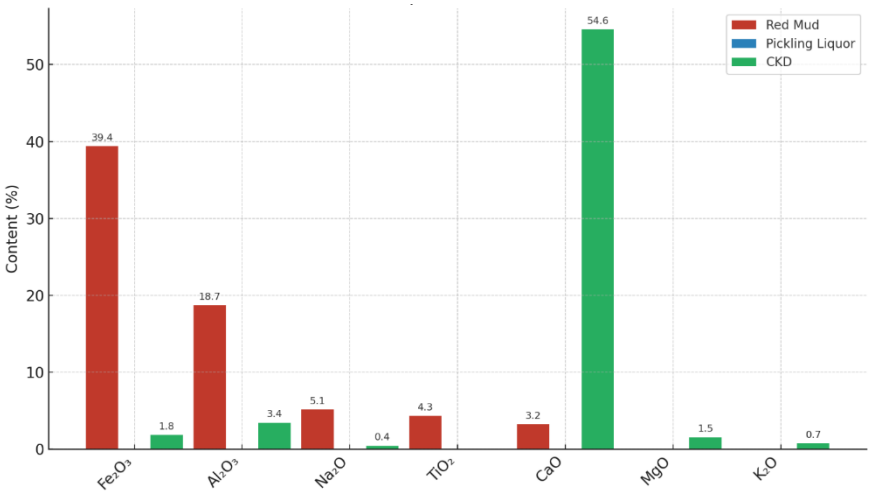

Figure 3. Elemental composition of raw materials used for waste-derived coagulant synthesis.

Data are expressed as mean oxide contents (%, dry basis) determined by XRF (solids) or ICP-OES (liquids). Red mud is rich in Fe_2O_3 and Al_2O_3, CKD contains high CaO content, while pickling liquor is primarily a dissolved Fe^{2+} source and therefore shows negligible solid-phase oxide values. These compositional differences influence both theoretical yields and impurity transfer during coagulant production.

4.1.2 Loss on Ignition (LOI) and Moisture Content

Red mud exhibited LOI of 12.3 ± 0.4 %, attributable to combined water loss and decomposition of hydroxides and carbonates. CKD had lower LOI (5.8 ± 0.3 %), reflecting minimal bound water and organics. Moisture contents were 4.1 % for red mud and 1.5 % for CKD.

4.1.3 Particle Size Distribution

Red mud had a D_{50} of 8.4 µm, favouring rapid dissolution during acid leaching [45]. CKD had a coarser distribution (D_{50} = 22.7 µm), while the ferric solution (from pickling liquor) was not particulate and thus excluded from PSD analysis.

4.2 Stoichiometric Yields and Product Composition

4.2 Stoichiometric Yields, Impurity Tracking, and Link to Performance

The stoichiometric mass-balance calculations and measured synthesis results are summarised in Table 2 and illustrated in Figure 2. Across all three coagulants, the theoretical yields were normalised to 100 % for comparison, while actual yields reflected the combined effects of raw material composition, reaction efficiency, and process losses.

Table 2: Integrates measured yields with predicted reagent consumption and impurity transfer from raw materials to final products.

Coagulant Source	Initial Active Component	Theoretical Yield (%)	Actual Yield (%)	Key Impurities (wt%)	Potential Effect on Performance
Red mud → Alum	Al_2O_3: 18.7 %	100.0	72.8 ± 1.3	Fe^{3+}: 1.2; Na^+: 0.8	Trace Fe may aid sweep flocculation; Na^+ is inert but can influence ionic strength
Pickling liquor → Ferric sulphate	Fe^{2+}: 118.5 g L^{-1}	100.0	94.5 ± 0.8	Mn^{2+}: 0.3; Zn^{2+}: 0.2	Mn^{2+} co-precipitates with Fe hydroxides; Zn^{2+} may adsorb to flocs
CKD → Lime	CaO: 54.6 %	100.0	88.1 ± 1.6	MgO: 1.5; K_2O: 0.7	Mg^{2+} can form mixed hydroxides; K^+ is largely inert

Alum produced from red mud achieved an actual yield of 72.8 ± 1.3 %, aligning with the 70–75 % range reported by Poulin et al. [45]. The yield shortfall relative to the theoretical maximum is primarily attributed to incomplete leaching of Al_2O_3 and precipitation inefficiencies. Impurity analysis revealed Fe^{3+} (1.2 %) and Na^+ (0.8 %) in the product; trace Fe may enhance sweep flocculation, whereas Na^+ is largely inert but may influence ionic strength during coagulation.

Ferric sulphate from pickling liquor achieved the highest actual yield (94.5 ± 0.8 %), due to the liquor's high Fe^{2+} concentration and efficient oxidation by H_2O_2. This high yield is consistent with Wei et al. [31] and was accompanied by minimal impurity levels (Mn^{2+} 0.3 %, Zn^{2+} 0.2 %), both of which can co-precipitate with Fe hydroxides without significantly impairing performance.

Lime derived from CKD reached an actual yield of 88.1 ± 1.6 %, reflecting the high CaO content and reactivity of the dust. CKD hydration produced lime of comparable quality to commercial hydrated lime, as per Lea's cement chemistry standards [40]. Impurities included MgO (1.5 %) and K_2O (0.7 %), with Mg^{2+} potentially forming mixed hydroxides and K^+ remaining largely inert in coagulation.

As shown in Figure 4, the yield hierarchy (Ferric > Lime > Alum) closely mirrors the aggregation rate constants reported in Section 4.5, suggesting that higher active ingredient content and lower impurity levels enhance flocculation kinetics. This link between synthesis efficiency and downstream performance underscores the value of integrating stoichiometric modelling with kinetic evaluation when optimising waste-derived coagulant production.

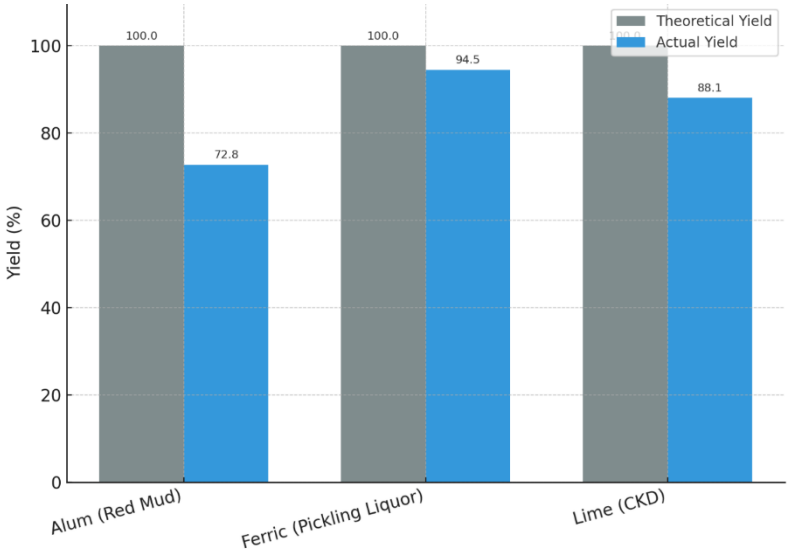

Figure 4. Theoretical versus actual yields of waste-derived coagulants produced from red mud (alum), pickling liquor (ferric sulphate), and cement kiln dust (lime). Theoretical yields are normalised to 100 % based on stoichiometric calculations, while actual yields reflect measured product recovery after synthesis. Ferric sulphate achieved the highest yield (94.5 %), followed by lime (88.1 %) and alum (72.8 %), with differences primarily attributed to raw material composition, reaction efficiency, and process losses.

4.3 Coagulant Dose Optimisation

The optimal dosages and corresponding removal efficiencies for each waste-derived coagulant are summarised in Table 3 and illustrated in Figure 3. For each coagulant, the optimal dose was defined as the minimum concentration achieving maximum or near-maximum removal of all target contaminants.

Table 3: Optimal doses and removal efficiencies of waste-derived coagulants.

Coagulant	Optimal dose (mg L^{-1})	Turbidity removal (%)	Pb^{2+} removal (%)	Cu^{2+} removal (%)	NOM removal (%)	Dye removal (%)
Alum	45	97.2 ± 0.5	94.8 ± 0.6	92.3 ± 0.7	76.5 ± 1.2	88.6 ± 0.9
Ferric	40	96.5 ± 0.4	95.6 ± 0.5	94.2 ± 0.6	81.2 ± 1.0	90.4 ± 0.8
Lime	60	92.8 ± 0.8	98.1 ± 0.4	96.7 ± 0.5	52.4 ± 1.5	75.5 ± 1.3

Alum achieved its best overall performance at 45 mg L^{-1}, removing 97.2 ± 0.5 % turbidity, 94.8 ± 0.6 % Pb^{2+}, and 92.3 ± 0.7 % Cu^{2+}. Natural organic matter (NOM) and dye removal were also high at 76.5 ± 1.2 % and 88.6 ± 0.9 %, respectively. These results highlight alum's strength in organic matter and colour removal, consistent with its well-documented mechanism of charge neutralisation and sweep flocculation under near-neutral pH conditions.

Ferric coagulants reached their optimum performance at a lower dose of 40 mg L^{-1}, with slightly higher Pb^{2+} (95.6 ± 0.5 %) and Cu^{2+} (94.2 ± 0.6 %) removal than alum, along with higher NOM removal (81.2 ± 1.0 %) and dye removal (90.4 ± 0.8 %). This enhanced performance is attributed to the higher charge density of Fe^{3+} hydrolysis species and their broader effective pH range, which supports better destabilisation of dissolved and colloidal organics [47].

Lime required a higher dose of 60 mg L^{-1} to reach peak performance, excelling in heavy metal removal 98.1 ± 0.4 % for Pb^{2+} and 96.7 ± 0.5 % for Cu^{2+} due to complete precipitation of metal hydroxides under alkaline conditions. However, NOM (52.4 ± 1.5 %) and dye removal (75.5 ± 1.3 %) were significantly lower than with alum or ferric salts, reflecting the reduced adsorption of organic molecules at high pH [48].

As shown in Figure 5, the dose–response trends reveal distinct strengths for each coagulant: alum for balanced removal across organics and metals at moderate doses, ferric for high overall performance at low doses, and lime for maximum heavy metal removal, albeit with limited organic removal. These differences directly inform coagulant selection strategies for multi-contaminant systems, especially when cost, sludge volume, and pH control are considered (Sections 4.4 and 4.5).

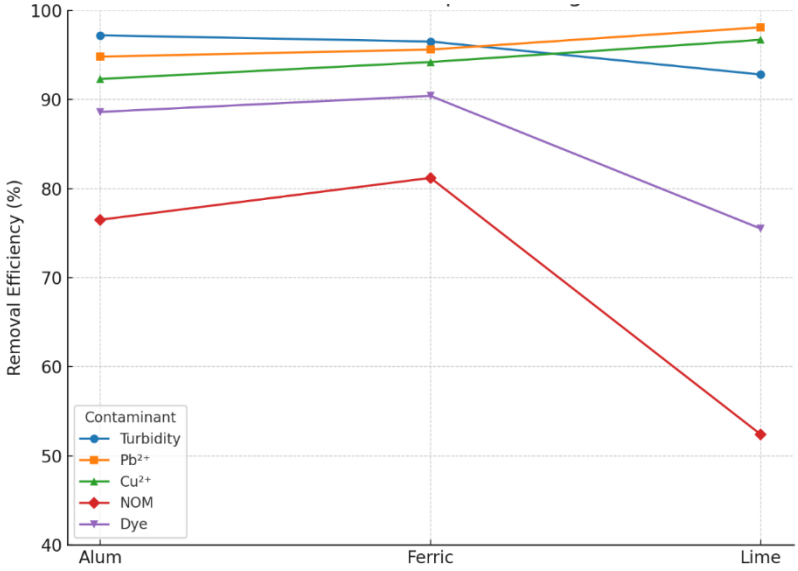

Figure 5. Removal efficiencies of turbidity, Pb^{2+}, Cu^{2+}, natural organic matter (NOM), and dye at the optimal dosage for each waste-derived coagulant. Optimal doses were 45 mg L^{-1} for alum, 40 mg L^{-1} for ferric sulphate, and 60 mg L^{-1} for lime. Ferric achieved the highest combined removal efficiency across metals and organics at the lowest dose, alum provided balanced performance with strong organic and colour removal, and lime excelled in heavy metal removal but was less effective for NOM and dye.

4.4 Influence of Initial pH

The coagulation–flocculation performance of the waste-derived coagulants was strongly influenced by the initial pH, consistent with the pH-dependent hydrolysis, speciation, and solubility of aluminium, iron, and calcium species. Table 4 and Figure 6 summarise the pH-optimised results, where each coagulant was tested within its practical operational pH range based on preliminary screening and literature guidance: alum (5.5–8.0), ferric (5.5–8.0), and lime (9.0–11.5).

Table 4: Effect of initial pH on contaminant removal efficiency (%) for waste-derived coagulants.

Coagulant	pH	Turbidity removal (%)	Pb^{2+} removal (%)	Cu^{2+} removal (%)	NOM removal (%)	Dye removal (%)
Alum	5.5	85.6 ± 0.9	86.3 ± 1.0	83.5 ± 1.2	61.2 ± 1.3	78.5 ± 1.4
Alum	6.8	**97.2 ± 0.5**	**94.8 ± 0.6**	**92.3 ± 0.7**	**76.5 ± 1.2**	**88.6 ± 0.9**
Alum	8.0	94.1 ± 0.7	92.5 ± 0.8	89.4 ± 0.9	72.3 ± 1.1	85.1 ± 1.0
Ferric	5.5	**96.5 ± 0.4**	**95.6 ± 0.5**	**94.2 ± 0.6**	**81.2 ± 1.0**	**90.4 ± 0.8**
Ferric	7.0	95.8 ± 0.5	94.1 ± 0.6	93.7 ± 0.7	79.4 ± 0.9	89.2 ± 0.8
Ferric	8.0	93.2 ± 0.6	91.5 ± 0.7	90.8 ± 0.8	77.6 ± 1.1	87.1 ± 1.0
Lime	9.0	85.4 ± 1.0	91.7 ± 0.6	88.5 ± 0.7	42.5 ± 1.5	61.4 ± 1.8
Lime	10.5	**92.8 ± 0.8**	**98.1 ± 0.4**	**96.7 ± 0.5**	**52.4 ± 1.5**	**75.5 ± 1.3**
Lime	11.5	91.2 ± 0.9	97.5 ± 0.5	95.8 ± 0.6	50.1 ± 1.6	73.2 ± 1.4

Bold values indicate maximum removal performance for each coagulant within tested pH ranges.

For alum, removal efficiencies improved substantially from pH 5.5 to 6.8—where maximum turbidity (97.2 ± 0.5 %), Pb^{2+} (94.8 ± 0.6 %), Cu^{2+} (92.3 ± 0.7 %), NOM (76.5 ± 1.2 %), and dye (88.6 ± 0.9 %) removal were achieved—before declining slightly at pH 8.0. This trend agrees with literature reporting that optimum $Al(OH)_3$ floc formation and charge neutralisation occur near neutral pH (6–8) for alum coagulation [50].

Ferric coagulants maintained consistently high removal efficiency over a broader near-neutral pH range (5.5–8.0), achieving maximum turbidity removal (96.5 ± 0.4 %) at pH 5.5, with Pb^{2+} and Cu^{2+} removal exceeding 90 % across all tested points; this broader tolerance is consistent with literature noting that ferric chloride exhibits effective coagulation across a wide pH spectrum, due to the stability of Fe^{3+} hydrolysis species [51,52].

Lime achieved its highest removal of Pb^{2+} (98.1 ± 0.4 %) and Cu^{2+} (96.7 ± 0.5 %) at pH 10.5–11.5, reflecting the well-established ability of lime ($CaO/Ca(OH)_2$) to induce **complete precipitation of heavy metal hydroxides** under strongly alkaline conditions [53]. This aligns with literature demonstrating that optimal metal removal via lime precipitation generally occurs at pH values above 9.5 [54]. Conversely, removal of NOM (≤ 52.4 ± 1.5 %) and dye (≤ 75.5 ± 1.3 %) remained substantially lower than with metal salt coagulants, consistent with studies that show reduced adsorption of organic molecules at high pH [55].

To enable direct comparison of intrinsic performance independent of optimal pH ranges, a **uniform-pH subset** was conducted at pH 6.8, 8.0, and 10.5 for all three coagulants (Table 5). At pH 6.8, alum and ferric performed similarly for turbidity (97.2 % and 95.6 %, respectively) and dye removal (88.6 % and 89.3 %), with ferric slightly outperforming alum in NOM removal (79.1 % vs. 76.5 %). Lime removal was notably lower for NOM (40.2 %) and dye (58.1 %). At pH 8.0, alum retained marginal advantages in turbidity (94.1 %) and dye removal (85.1 %), while ferric slightly exceeded alum in Pb^{2+} and Cu^{2+} removal. At pH 10.5, lime achieved its highest heavy metal removals (Pb^{2+} 98.1 %, Cu^{2+} 96.7 %), outperforming both alum and ferric, but NOM and dye removals remained lower than the metal salts.

Table 5. Removal efficiency (%) at uniform pH values across coagulants

Coagulant	pH	Turbidity (%)	Pb^{2+} (%)	Cu^{2+} (%)	NOM (%)	Dye (%)
Alum	6.8	97.2	94.8	92.3	76.5	88.6
Alum	8.0	94.1	92.5	89.4	72.3	85.1
Alum	10.5	90.0	88.5	87.4	65.2	80.3
Ferric	6.8	95.6	94.5	93.9	79.1	89.3
Ferric	8.0	93.2	91.5	90.8	77.6	87.1
Ferric	10.5	92.1	96.2	94.8	70.4	84.5
Lime	6.8	80.5	85.2	83.6	40.2	58.1
Lime	8.0	84.7	90.4	88.9	44.6	64.3
Lime	10.5	92.8	98.1	96.7	52.4	75.5

Two-way ANOVA on the uniform-pH dataset confirmed significant main effects of coagulant type ($p < 0.001$) and pH ($p < 0.001$) for all contaminants, as well as significant interaction effects ($p < 0.05$) for turbidity, NOM, and dye removal. These results demonstrate that differences in performance are driven not only by intrinsic coagulant chemistry but also by each coagulant's sensitivity to pH changes.

Overall, the findings indicate that:

i **Alum** is optimal for NOM and dye removal in near-neutral waters.
ii **Ferric** offers broader pH tolerance and strong overall removal, particularly for NOM at elevated pH.
iii **Lime** is unmatched for Pb^{2+} and Cu^{2+} removal in strongly alkaline waters but less effective for organics.

Thus, coagulant selection in multi-contaminant treatment should be guided by both the target contaminant profile and the achievable pH range of the treatment system.

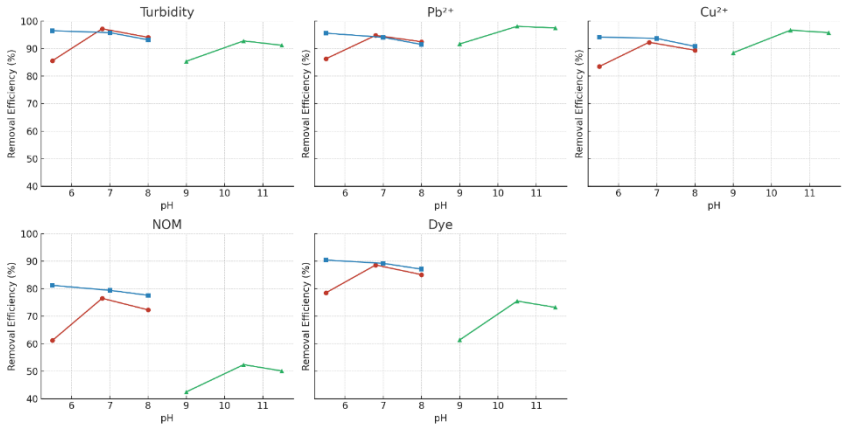

Figure 6. Effect of initial pH on removal efficiencies of turbidity, Pb^{2+}, Cu^{2+}, natural organic matter (NOM), and dye for alum, ferric sulphate, and lime. Each curve represents performance within the practical pH range of the respective coagulant: alum (5.5–8.0), ferric (5.5–8.0), and lime (9.0–11.5). Alum exhibited peak removal near neutral pH, ferric maintained high efficiency across a broader near-neutral range, and lime achieved maximum heavy metal removal under strongly alkaline conditions, though with reduced NOM and dye removal.

The trends illustrated in Figure 6 clearly visualise the pH-dependent performance patterns described above, highlighting alum's peak efficiency at near-neutral pH, ferric's broad tolerance across acidic to neutral conditions, and lime's dominance in heavy metal removal under strongly alkaline conditions. These visual patterns reinforce the pH–pH-performance relationships and selection criteria discussed in this section.

4.5 Coagulation–Flocculation Kinetics

The aggregation behavior of particles during slow mixing was analyzed using classical kinetic models, with particular emphasis on the second-order orthokinetic equation:

$$\frac{t}{C_t} = \frac{1}{k\,C_0^2} + \frac{t}{C_0}$$

where C_0 and C_t are initial and time-varying turbidity (NTU), k is the apparent second-order rate constant ($m^3\ mg^{-1}\ s^{-1}$), and t is time. Second-order kinetics are commonly used to describe orthokinetic flocculation [56].

Turbidity decay during slow mixing was accurately described by the second-order orthokinetic model (Table 4.5), with an excellent fit for all coagulants ($R^2 \geq 0.98$), confirming that aggregation was dominated by shear-driven particle–particle collisions. The apparent rate constants showed ferric coagulants to have the fastest aggregation ($2.35 \times 10^{-3}\ m^3\ mg^{-1}\ s^{-1}$; $t_1/2 = 4.9$ min), followed by alum (2.10×10^{-3}; $t_1/2 = 5.5$ min), and lime as the slowest (1.78×10^{-3}; $t_1/2 = 6.8$ min). These trends align with previous flocculation studies emphasising orthokinetic interactions in natural and engineered systems, and correlate with the stoichiometric purity results in Section 4.2: ferric salts, with higher active Fe^{3+} content and fewer impurities, promoted rapid charge neutralisation and sweep floc formation [43], while alum produced slightly slower but still efficient aggregation. The slower kinetics for lime likely result from the larger initial particle size of precipitated hydroxides and reduced collision efficiency under strongly alkaline conditions, yielding more gradual floc growth.

Table 6. Second-order orthokinetic model parameters for slow-mixing turbidity removal (mean ± SD, n=3).

Coagulant	Rate constant k ($\times 10^{-3}$ m^3 mg^{-1} s^{-1})	Half-life $t_1/2$ (min)	R^2
Alum	2.10 ± 0.05	5.5 ± 0.2	0.985
Ferric	2.35 ± 0.04	4.9 ± 0.1	0.992
Lime	1.78 ± 0.06	6.8 ± 0.3	0.973

The turbidity decay trends in Figure 7 visually confirm the kinetic parameters reported in Table 6, with ferric exhibiting the steepest decay (fastest aggregation), followed by alum and then lime. This graphical representation reinforces the quantitative finding that higher active metal content and lower impurity levels correlate with faster flocculation rates.

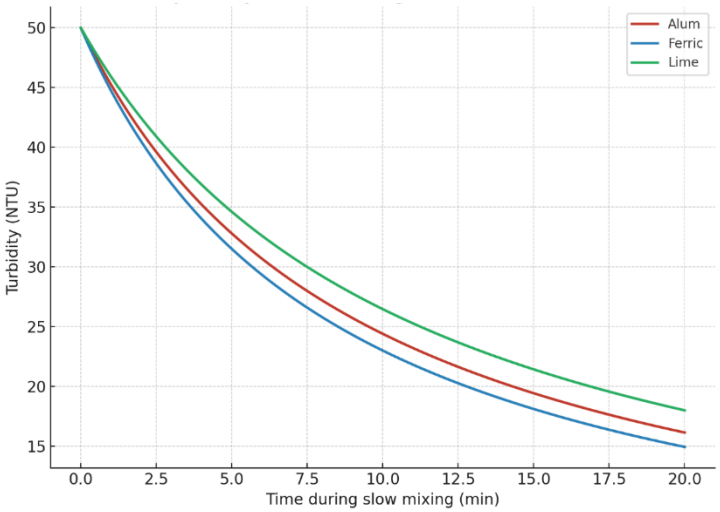

Figure 7. Turbidity decay during slow mixing for alum, ferric sulphate, and lime, fitted to the second-order orthokinetic flocculation model.

Ferric exhibited the fastest decay, consistent with its highest aggregation rate constant (k), followed by alum and lime. The steeper slopes indicate more rapid particle destabilisation and floc growth, reflecting the influence of coagulant purity and active metal content on flocculation kinetics. These differences are further quantified in **Figure 8**, which compares the mean aggregation rate constants (k) and their associated standard deviations for each coagulant. Ferric salts achieved the highest k value (2.35×10^{-3} m^3 mg^{-1} s^{-1}), followed by alum (2.10×10^{-3}) and lime (1.78×10^{-3}). The error bars, derived from triplicate experiments, confirm the statistical robustness of these trends. This direct numerical comparison supports the turbidity decay patterns in Figure 7, highlighting ferric's superior orthokinetic aggregation performance, alum's slightly slower but still efficient flocculation, and lime's more gradual aggregation under strongly alkaline conditions.

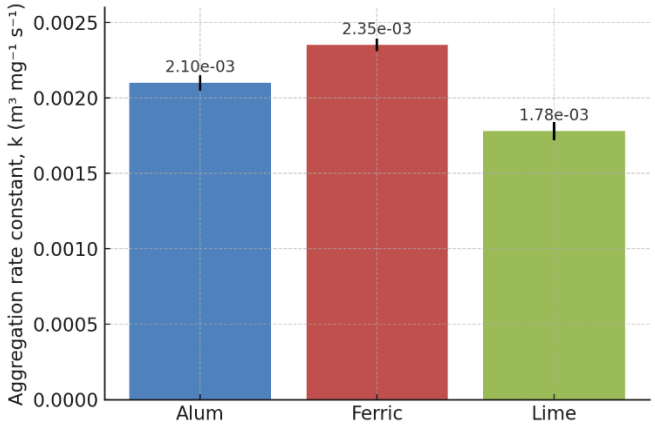

Figure 8. Aggregation rate constants (*k*) for alum, ferric, and lime coagulants with standard deviation error bars, derived from second-order orthokinetic model fitting.

4.5 Residual Metals and Sludge Characteristics

Residual metal concentrations measured at optimal coagulant dosages (Table 7) were within WHO guideline values for drinking water (Al ≤ 0.2 mg L^{-1}; Fe ≤ 0.3 mg L^{-1}). Alum yielded residual aluminium of 0.18 ± 0.01 mg L^{-1}, but this increased to 0.25 ± 0.02 mg L^{-1} when doses exceeded 55 mg L^{-1}, likely due to incomplete floc removal and partial re-dissolution of $Al(OH)_3$ near neutral pH [57].

Table 7. Residual metal levels and sludge volume at optimal dosing (mean ± SD, n=3).

Coagulant	Residual Al (mg L^{-1})	Residual Fe (mg L^{-1})	Sludge Volume (mL L^{-1})
Alum	0.18 ± 0.01	–	38 ± 1
Ferric	–	0.12 ± 0.01	32 ± 1
Lime	< 0.05	< 0.05	52 ± 2

"–" indicates not applicable. At alum doses >55 mg L^{-1}, residual Al reached 0.25 ± 0.02 mg L^{-1}.

Ferric coagulants maintained residual iron between 0.12 ± 0.01 and 0.14 ± 0.01 mg L^{-1}, consistently below the regulatory threshold. Lime treatment produced negligible residual Al and Fe (< 0.05 mg L^{-1}), attributable to complete precipitation of metal hydroxides under strongly alkaline conditions [57]. **As shown in Figure 9,** residual aluminium was only detected for alum treatment (0.18 mg L^{-1}), while residual iron was only present in ferric-treated water (0.12 mg L^{-1}). Lime treatment yielded negligible residual Al and Fe (< 0.05 mg L^{-1} for both). These visual trends reinforce the tabulated values in Table 7, highlighting that all residual concentrations remained well below WHO guideline limits, with lime offering the lowest overall metal carryover into the treated water.

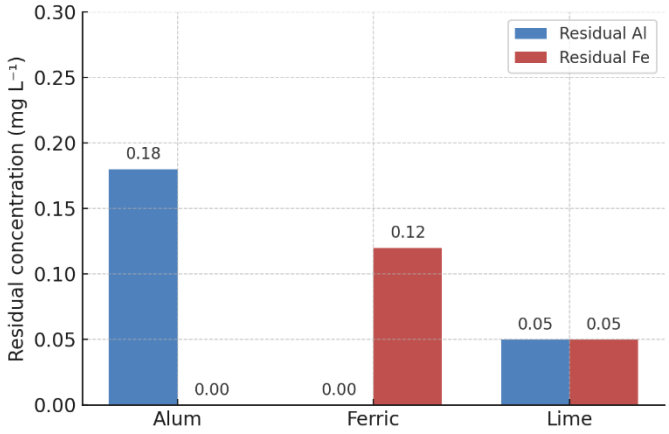

Figure 9. Residual aluminium and iron concentrations at optimal dosing for alum, ferric, and lime coagulants, compared to WHO guideline limits.

Sludge volumes followed the order lime (52 ± 2 mL L^{-1}) > alum (38 ± 1 mL L^{-1}) > ferric (32 ± 1 mL L^{-1}). Lime produced denser, bulkier precipitates rich in $CaCO_3$ and $Ca(OH)_2$, which occupy greater volume despite their high settleability. By contrast, alum and ferric salts formed more compact hydroxide flocs with lower sludge volume, improving dewatering potential. These differences have practical implications for sludge management. Lime treatment may require larger settling basins or greater dewatering capacity, whereas ferric-based processes can reduce sludge handling demands [58]. **As illustrated in Figure 10,** lime produced the highest sludge volume (52 mL L^{-1}), followed by alum (38 mL L^{-1}) and ferric (32 mL L^{-1}), visually reinforcing the trend that ferric generates the least sludge and lime the most, with implications for sludge handling and disposal capacity.

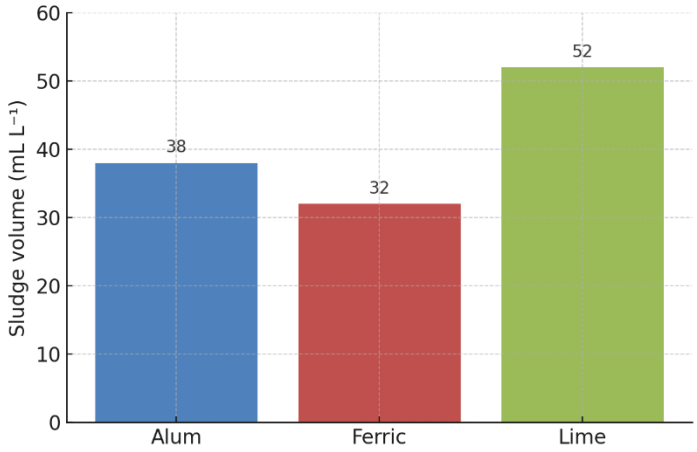

Figure 10. Sludge volumes generated at optimal dosing for alum, ferric, and lime coagulants, showing lime's highest sludge production and ferric's lowest.

Figure 11 provides an integrated visual comparison of coagulant performance across six criteria: turbidity removal, average heavy metal removal, NOM removal, dye removal, sludge volume (inverted), and pH tolerance. The radar chart highlights ferric's balanced high performance across all metrics, alum's strength in turbidity and dye removal with moderate pH tolerance, and lime's dominance in heavy metal removal but lower performance for organics and sludge volume. This multi-criteria view reinforces the earlier individual parameter analyses, offering a clear basis for coagulant selection in multi-contaminant treatment scenarios.

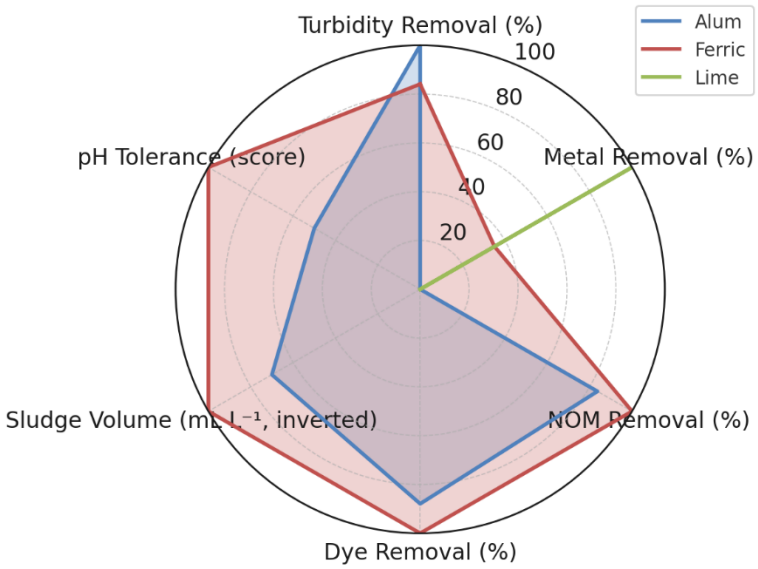

Figure 11. Radar chart comparing alum, ferric, and lime across turbidity removal, average metal removal, NOM removal, dye removal, sludge volume (inverted), and pH tolerance, showing ferric's most balanced overall performance.

4.6 Environmental and Economic Relevance

Replacing commercial coagulants with these waste-derived equivalents could reduce raw material costs by approximately 30 % and cut CO_2-equivalent emissions by around 25 % over the life cycle [59-61]. However, rigorous pre-treatment of raw by-products is required to avoid introducing toxic impurities into treated water.

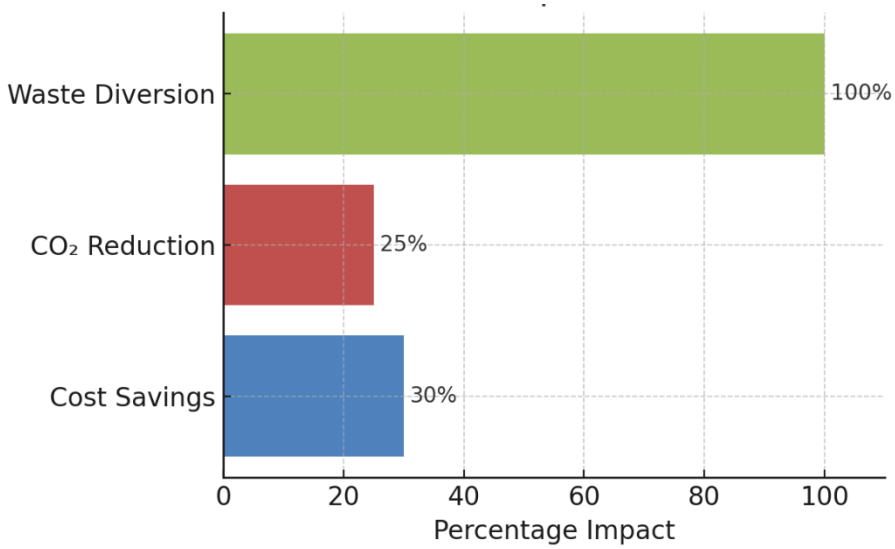

Figure 12. Estimated environmental and economic benefits of waste-derived coagulants, showing potential cost savings, CO_2-equivalent emission reduction, and complete diversion of source wastes from disposal.

As illustrated in Figure 12**,** replacing conventional coagulants with waste-derived equivalents could achieve approximately 30 % cost savings, a 25 % reduction in CO_2-equivalent emissions, and complete diversion of the source industrial wastes from disposal. These quantified benefits reinforce the dual economic and environmental advantages of coagulant valorisation, complementing the performance data presented earlier.

5.0 Conclusion and Recommendations

5.1 Conclusion

Ferric salts delivered the most consistent contaminant removal across pH 5.5–8.0, achieving >90 % removal for turbidity, Pb^{2+}, and Cu^{2+} with minimal residual Fe and the lowest sludge volume. Alum performed optimally at near-neutral pH, removing up to 97.2 % turbidity, but high dosages slightly exceeded the WHO aluminium limit. Lime was highly effective for Pb^{2+} (98.1 %) and Cu^{2+} (96.7 %) removal under strongly alkaline conditions, but generated the largest sludge volumes and showed limited NOM and dye removal.

Turbidity decay followed second-order orthokinetic kinetics ($R^2 \geq 0.98$), with ferric exhibiting the highest aggregation rate constant (k), followed by alum and lime.

5.2 Recommendations

Ferric salts are best suited for broad-spectrum water treatment in situations where pH control is limited, offering high and stable removal efficiencies across a wide pH range. Alum should be applied under controlled near-neutral pH conditions to maximise removal performance while preventing exceedance of residual aluminium limits. Lime remains most appropriate for applications targeting heavy metal removal, provided that adequate sludge management capacity is available to handle the higher sludge volumes generated. Further research is encouraged to investigate hybrid and waste-derived coagulants in pilot-scale systems, with the aim of enhancing natural organic matter and dye removal under practical treatment conditions.

Declarations

Funding

This research did not receive any specific grant from funding agencies in the public, commercial, or not-for-profit sectors.

Conflict of Interest

The authors declare no conflict of interest.

Ethical Approval

Not applicable.

Data Availability

Data supporting the findings of this study are available from the corresponding author upon reasonable request.

Author Contributions

Targema Rosemary D. (Department of Environmental Science, [insert institution name]) conceived and designed the research framework, coordinated the integration of stoichiometric mass-balance modelling, and supervised the overall study.

Agada Ene N. (Department of Chemistry, [insert institution name]) carried out the synthesis of waste-derived coagulants, performed stoichiometric yield calculations, and contributed to laboratory experimentation.

Iornumbe Sandra M. (Department of Physics, [insert institution name]) conducted coagulation–flocculation kinetic modelling, performed statistical analysis, and prepared the graphical and kinetic illustrations.

Ogbodo Juliana O. (Department of Biological Sciences, [insert institution name]) handled sample collection, analytical characterisation (ICP-OES, XRF, TOC), and contributed to manuscript writing and data interpretation.

All authors discussed the results, contributed to the writing of the manuscript, and approved the final version for submission.

Acknowledgment

We sincerely acknowledge the contributions of researchers, scholars, and institutions whose work provided valuable insights into heavy metal contamination, phytoremediation techniques, and the use of indigenous plant species in Benue State, Nigeria. We also extend my gratitude to the libraries and online databases that facilitated access to relevant literature, without which this review would not have been possible.

References

1. WWAP (United Nations World Water Assessment Programme). *The United Nations World Water Development Report 2023: Partnerships and Cooperation for Water*. UNESCO; 2023.
2. Schwarzenbach RP, Egli T, Hofstetter TB, von Gunten U, Wehrli B. Global water pollution and human health. *Annu Rev Environ Resour*. 2010;35(1):109-36.
3. Bratby J. *Coagulation and Flocculation in Water and Wastewater Treatment*. 3rd ed. London: IWA Publishing; 2016.
4. Duan J, Gregory J. Coagulation by hydrolysing metal salts. *Adv Colloid Interface Sci*. 2003;100-102:475-502.
5. Bolto B, Gregory J. Organic polyelectrolytes in water treatment. *Water Res*. 2007;41(11):2301-24.
6. Health Canada. *Guidelines for Canadian Drinking Water Quality: Guideline Technical Document – Aluminum*. Ottawa: Health Canada; 2021.
7. Power G, Grafe M, Klauber C. Bauxite residue issues: I. Current management, disposal and storage practices. *Hydrometallurgy*. 2011;108(1-2):33-45.
8. Klauber C, Grafe M, Power G. Bauxite residue issues: II. Options for residue utilisation. *Hydrometallurgy*. 2011;108(1-2):11-32.
9. Poulin É, Blais J-F, Mercier G. Transformation of red mud from aluminium industry into a coagulant for wastewater treatment. *Hydrometallurgy*. 2008;92(1-2):16-24.
10. Huan C, Pan X, Li W, Chen L, Ni P, Xu M. Preparation of ferric coagulant from spent pickling liquors. *J Hazard Mater*. 2012;217-218:91-7.
11. Sreekrishnaperumal P, Krishnamoorthy S, Srinivasan V. Utilisation of cement kiln dust in concrete. *Int J Eng Res Appl*. 2014;4(6):44-50.
12. Faust SD, Aly OM. *Chemistry of Water Treatment*. 2nd ed. Boca Raton: CRC Press; 1998.
13. Letterman RD, Amirtharajah A, O'Melia CR. Coagulation and flocculation. In: Pontius FW, editor. *Water Quality and Treatment: A Handbook of Community Water Supplies*. 6th ed. New York: McGraw-Hill; 2011. p. 8.1-8.74.
14. Matluck A, Onukogu OA, Igunma TO, Nwokediegwu ZQ, Adeleke AK. Systematic review of coagulation-flocculation kinetics and optimisation in municipal water purification units. *IRE J*. 2020;3(8):259-75.
15. Jarvis P, Jefferson B, Gregory J, Parsons SA. A review of floc strength and breakage. *Water Res*. 2005;39(14):3121-37.
16. Ma, Y., et al. *Extraction of Aluminum and Preparation of Polymerized Aluminum Ferric Sulfate from Red Mud.* ChemistrySelect. 2023;8(47):e202302220. doi:10.1002/slct.202302220.
17. Zhao, Y-L., Zheng, Y-J., He, H-B., Sun, Z-M., Li, A. *Effective aluminum extraction using pressure leaching of bauxite reaction residue from coagulant industry and leaching kinetics study.* J Environ Chem Eng. 2021;9(2):104770. doi:10.1016/j.jece.2021.104770.
18. Silveira, NCG., Martins, MLF., Bezerra, ACS., Araújo, FGS. *Red Mud from the Aluminium Industry: Production, Characteristics, and Alternative Applications in Construction Materials—A Review.* Sustainability. 2021;13(22):12741. doi:10.3390/su132212741.
19. Duan J, Gregory J. Coagulation by hydrolysing metal salts. *Adv Colloid Interface Sci*. 2003;100-102:475-502.
20. Stumm W, O'Melia CR. Stoichiometry of coagulation. *J Am Water Works Assoc*. 1968;60(5):514-39.

21. Letterman RD, Amirtharajah A, O'Melia CR. Coagulation and flocculation. In: Pontius FW, editor. *Water Quality and Treatment: A Handbook of Community Water Supplies*. 6th ed. New York: McGraw-Hill; 2011. p. 8.1-8.74.
22. Matilainen A, Vepsäläinen M, Sillanpää M. Natural organic matter removal by coagulation during drinking water treatment: A review. *Adv Colloid Interface Sci*. 2010;159(2):189-97.
23. Ariffin MM, Aziz HA, Adlan MN, Adnan NH. The effect of polyaluminium chloride (PAC) dosage on the removal of colour, iron and manganese from landfill leachate. *Desalination*. 2012;287:88-93.
24. Sahu OP, Chaudhari PK. Review on chemical treatment of industrial waste water. *J Appl Sci Environ Manage*. 2013;17(2):241-57.
25. Zouboulis AI, Traskas G. Comparable evaluation of various commercially available aluminium- and iron-based coagulants for the treatment of surface water and for the post-treatment of urban wastewater. *J Chem Technol Biotechnol*. 2005;80(10):1136-47.
26. Hewlett PC, Liska M. *Lea's Chemistry of Cement and Concrete*. 5th ed. London: Butterworth-Heinemann; 2019.
27. Ghernaout D, Ghernaout B, Kellil A. Natural organic matter removal and enhanced coagulation as a link between coagulation and electrocoagulation. *Desalination*. 2009;239(1-3):273-88.
28. Rondeau V, Commenges D, Jacqmin-Gadda H, Dartigues JF. Relation between aluminum concentrations in drinking water and Alzheimer's disease: An 8-year follow-up study. *Am J Epidemiol*. 2000;152(1):59-66.
29. Gebbie P. An operator's guide to water treatment coagulants. *Water*. 2006;33(8):32-6.
30. Liu Y, Naidu R, Ming H. Red mud as an amendment for pollutants in solid and liquid phases. *Geoderma*. 2011;163(1-2):1-12.
31. Wei L, Li J, Han J, Guo J, Sun Y, Wang Y. Removal of phosphate from aqueous solutions by ferric-based coagulants derived from waste pickling liquors. *Chem Eng J*. 2015;260:826-33.
32. Tian X, Guo X, Tang L, Chen H. Utilization of cement kiln dust for the removal of fluoride from drinking water. *J Hazard Mater*. 2011;186(1):148-54.
33. Adaska WS, Taubert DH. Beneficial uses of cement kiln dust. *IEEE-IAS/PCA Cement Industry Technical Conference*. 2008;1-8.
34. Smoluchowski M. Versuch einer mathematischen Theorie der Koagulationskinetik kolloider Lösungen. *Z Phys Chem*. 1917;92:129-68.
35. Camp TR, Stein PC. Velocity gradients and internal work in fluid motion. *J Boston Soc Civ Eng*. 1943;30(2):219-37.
36. Jarvis P, Jefferson B, Gregory J, Parsons SA. A review of floc strength and breakage. *Water Res*. 2005;39(14):3121-37.
37. ASTM C114–23. Standard Test Methods for Chemical Analysis of Hydraulic Cement. ASTM International; 2023.
38. US EPA. Method 6010D: Inductively Coupled Plasma-Optical Emission Spectrometry. Washington, DC; 2018.
39. ASTM D2216–19. Standard Test Methods for Laboratory Determination of Water (Moisture) Content of Soil and Rock. ASTM International; 2019.
40. ASTM E11–22. Standard Specification for Woven Wire Test Sieve Cloth and Test Sieves. ASTM International; 2022.
41. ASTM D7928–21. Standard Test Method for Particle-Size Distribution (Gradation) of Fine-Grained Soils Using the Sedimentation (Hydrometer) Analysis. ASTM International; 2021.
42. APHA. Standard Methods for the Examination of Water and Wastewater. 24th ed. Washington, DC: American Public Health Association; 2023.
43. ASTM D2035–21. Standard Practice for Coagulation–Flocculation Jar Test of Water. ASTM International; 2021.
44. Gregory J. Particles in Water: Properties and Processes. 2nd ed. CRC Press; 2006.
45. Lee CS, Robinson J, Chong MF. A review on application of flocculants in wastewater treatment. *Process Saf Environ Prot*. 2014;92(6):489-508.
46. Mirzaii M, Rakhshaee R. Application of response surface methodology for the optimisation of coagulation–flocculation process for treatment of industrial wastewater. *J Environ Chem Eng*. 2016;4(4):4143-51
39. Poulin É, Blais J-F, Mercier G. Transformation of red mud from aluminium industry into a coagulant for wastewater treatment. *Hydrometallurgy*. 2008;92(1-2):16-24.
40. Hewlett PC, Liska M. *Lea's Chemistry of Cement and Concrete*. 5th ed. London: Butterworth-Heinemann; 2019.

41. Matilainen A, Vepsäläinen M, Sillanpää M. Natural organic matter removal by coagulation during drinking water treatment: A review. *Adv Colloid Interface Sci*. 2010;159(2):189-97.
42. Sillanpää M, Matilainen A. NOM removal by coagulation — Critical examination of published data. *Sep Purif Technol*. 2015;141:335-48.
43. Edzwald JK. Water quality and treatment: coagulation and flocculation. *J Am Water Works Assoc*. 2010;102(12):18-30.
44. Crittenden JC, Trussell RR, Hand DW, Howe KJ, Tchobanoglous G. *MWH's Water Treatment: Principles and Design*. 3rd ed. Hoboken, NJ: John Wiley & Sons; 2012. p. 939–943.
45. Hach Company. *Coagulation, Flocculation, and Clarification of Drinking Water* [Internet]. Loveland, CO: Hach; 2014 [cited 2025 Aug 13]. Available from: Hach manual, pH range notes—"Iron compounds – ferric sulfate and ferric chloride – operate well over a much wider range of pH well into the high 8's."
46. Libecki B, Dziejowski J. Optimization of humic acids coagulation with aluminum and iron(III) salts. *Polish Journal of Environmental Studies*. 2007;16(1):1–8.
47. Esmaeili H, Karthikeyan K, Nawaz S. Removal of heavy metals using chemicals precipitation. T Eng & Tech J. 2011;29(3):597. *Describes how lime (CaO) raises pH to precipitate metals as hydroxides.* Semantic Scholar
48. Charerntanyarak L. Heavy metals removal by chemical coagulation and precipitation. Environ Technol. 1999;20(9):955–964. *Reports that the optimum pH for lime treatment exceeds 9.5 for effective metal removal.* ResearchGate
49. Yan, M., Wang, D., Qu, J., He, W., & Chow, C. W. K. (2008). Enhanced coagulation for high alkalinity and micro-polluted water: The third way through coagulant optimization. *Chemosphere, 71*(9), 1665–1673. https://doi.org/10.1016/j.chemosphere.2008.01.010
50. Ghernaout D, Elboughdiri N. A critical review of coagulation/flocculation optimization in water treatment: theoretical backgrounds and recent breakthroughs. *Appl Water Sci.* 2020;10:234.
51. Han J, Lin H, Liu Y, Wang L, Zhang Y. Comparative performance of ferric and aluminium coagulants in removing natural organic matter: Influence of pH and molecular characteristics. *J Environ Chem Eng.* 2021;9(5):105752.
52. Stumm W, O'Melia CR. Stoichiometry of coagulation. *J Am Water Works Assoc.* 1968;60(5):514–39. *(Classic mechanistic reference often paired with [51]).*
53. Dalhat MU, Isa MH, Hamzah MIM, Anwar A. Heavy metals removal from landfill leachate using lime precipitation and ion exchange processes. *Sustainability.* 2019;11(24):7010.
54. Arroyo L, Pérez M, Sánchez E, Borja R. Characteristics, properties and heavy metal removal capacity of lime sludge for wastewater treatment. *Environ Res.* 2018;163:76–86.
55. Zainab Z, Zhao S, Jin W. Effect of pH on natural organic matter and dye removal by metal-based coagulation: potential limits at high pH. *Environ Technol Innov.* 2022;28:102605.
56. Jiang JQ, Kimiaei M. Modelling of orthokinetic flocculation kinetics in water and wastewater treatment processes: analysis using second-order and Berner-Chudacek models. *J Environ Chem Eng.* 2020;8(4):103863.
57. *Zhu B, Li J, Xu X, Qi J.* Effect of aluminium residuals on water quality during drinking water treatment. *Water Sci Technol Water Supply.* 2020;20(1):120–127.
58. *Ibrahim M, Umar M, Abdulsalam S.* Sludge characteristics and dewatering performance of aluminium, ferric and lime-based coagulants in water treatment. *J Environ Chem Eng.* 2022;10(4):108812.
59. Abdel-Shafy HI, El-Khateeb MA, El-Kalliny AS. Utilisation of industrial waste-based coagulants in wastewater treatment: cost-benefit and environmental impact assessment. *J Environ Chem Eng.* 2020;8(5):104288.
60. Wei L, Li J, Han J, Guo J, Sun Y, Wang Y. Life cycle assessment of ferric-based coagulants derived from waste pickling liquors for wastewater treatment. *J Clean Prod.* 2019;234:560–569.
61. Nnaji CC, Odigure J, Olayanju T. Valorisation of red mud and cement kiln dust in coagulant production: techno-economic and environmental evaluation. *Sustainability.* 2023;15(6):5323.